Taylor & Francis
Taylor & Francis Group

RESEARCH ARTICLE

Combination prostate cancer therapy: Prostate-specific membranes antigen targeted, pH-sensitive nanoparticles loaded with doxorubicin and tanshinone

Guanxing Sun[a], Kai Sun[b] and Jie Sun[b]

[a]Department of Oncology, Municipal Hospital of Zaozhuang, Zaozhuang, P. R. China; [b]Department of Pharmacy, Municipal Hospital of Zaozhuang, Zaozhuang, P. R. China

ABSTRACT

Prostate cancer is the second most frequently diagnosed cancer in the men population. Combination anticancer therapy using doxorubicin (DOX) and another extract of traditional Chinese medicine is one nano-sized drug delivery system promising to generate synergistic anticancer effects, maximize the treatment effect, and overcome multi-drug resistance. The purpose of this study is to construct a drug delivery system for the co-delivery of DOX and tanshinones (TAN). Lipid nanoparticles loaded with DOX and TAN (N-DOX/TAN) were prepared by emulsification and solvent-diffusion method. PSMA targeted nanoparticles loaded with DOX and TAN (P-N-DOX/TAN) were synthesized by conjugating a PSMA targeted ligand to N-DOX/TAN. We evaluate the performance of this system *in vitro* and *in vivo*. P-N-DOX/TAN has a size of 139.7 ± 4.1 nm and a zeta potential of 11.2 ± 1.6 mV. The drug release of DOX and TAN from P-N-DOX/TAN was much faster than that of N-DOX/TAN. N-DOX/TAN presented more inhibition effect on tumor growth than N-DOX and N-TAN, which is consistent with the synergistic results and successfully highlighting the advantages of combing the DOX and TAN in one system. P-N-DOX/TAN achieved higher uptake by LNCaP cells ($58.9 \pm 1.9\%$), highest tumor tissue distribution, and the most significant tumor inhibition efficiency. The novel nanomedicine offers great promise for the dual drug delivery to prostate cancer cells, showing the potential of synergistic combination therapy for prostate cancer.

Introduction

Prostate cancer (PCa) is the most commonly diagnosed malignancy in men and is the second leading cause of cancer-related death among men in western society (Center et al., 2012; Siegel et al., 2012; Karantanos et al., 2013). Androgen deprivation therapy (ADT, surgical castration or medical castration) is the standard first-line therapy for patients with locally advanced PCa or metastatic PCa (Karantanos et al., 2013). However, the overwhelming majority of patients with advanced PCa eventually stop responding to traditional ADT and evolve into castration-recurrent PCa (CRPC) (Holzbeierlein et al., 2004; Mohler et al., 2004). As different disease progressions need different therapeutic treatments, CRPC has presented significant challenges to clinicians. Therefore, there is an urgent need for further research to resolve this clinical difficulty and change the paradigm of CRPC treatment.

Doxorubicin (DOX) is one of the most widely used antitumor drugs in PCa (SreeHarsha et al., 2019), but its significant side effects and non-selectivity are major disadvantages (Li, Xie, et al., 2019). At present, the research focus on nano-sized drug delivery systems is to improve the efficacy of chemotherapy and solve the problem of biocompatibility,

examples included Zhang et al. developed DOX loaded nanostructured lipid carriers for prostate cancer (Zhang, Dang, et al., 2017). Tambe et al. also developed DOX contained silica nanoparticles to enhance the apoptotic effect in prostate cancer cells (Tambe et al., 2018). DOX was also co-loaded with other drugs, including docetaxel and simvastatin within nanocarriers for prostate cancer therapy (Li, Xie, et al., 2019; Li, Zhan, et al., 2019). Tanshinones (TAN) are purified from the traditional Chinese herb *Salvia miltiorrhiza Bunge* (Danshen) and were reported to inhibit the growth of PCa cells and suspend the growth of prostate tumor in mice (Ketola et al., 2016; Wang et al., 2019). In this study, TAN was used in combination with DOX.

Two characteristics of PCa that can be utilized for the design of a targeted drug delivery system are over-expressed prostate-specific membrane antigen (PSMA) (Argenziano et al., 2018; Autio et al., 2018). PSMA is a cell surface protein that is a well-established tumor marker including prostate cancers but not present on healthy tissue vasculature (Silver et al., 1997; Chang et al., 1999). Its expression level is higher in CRPC than in early PCa (Wang et al., 2014). Thus, PSMA has been an attractive target for PCa, especially CRPC targeted drug delivery. Also, pH-responsive drug delivery

CONTACT Jie Sun ✉ sunjiemhzz@163.com 📍 Department of Pharmacy, Municipal Hospital of Zaozhuang, No.41, Longtou Road, Zaozhuang 277100, P. R. China.

systems are mostly intended to release drugs in the tumor site, which is far more acidic than the wider physiological environment (Xu et al., 2018; Cao et al., 2019). In the present study, we designed dual responsive drug delivery systems to co-delivery DOX and TAN.

In summary, the nano-sized delivery system is constructed as follows: (1) DSPE-PEG and lipids were applied as materials to carry DOX and TAN; (2) PSMA targeted ligand was selected as the surface modifier; (3) a pH-sensitive adipic acid dihydrazide (HZ) was chosen to conjugate the PSMA targeted ligand with the PEG end. We evaluate the performance of this system *in vitro* and *in vivo*.

Materials and methods

Materials

DOX, TAN, and coumarin-6 (C-6) were purchased from Sigma-Aldrich (St. Louis, MO). 1,2-distearoyl-sn-glycero-3-phosphoethanolamine-N-[succinyl(polyethylene glycol)-2000]-adipic acid dihydrazide (DSPE-PEG-HZ) and soya bean lecithin (SBL) were provided by Shanghai Ponsure Biotech, Inc (Shanghai, China). (2-(3-[1-carboxy-5-[7-(2,5-dioxopyrrolidin-1-yloxycarbonyl)heptanoylamino]pentyl]-ureido)pentanedioic acid (P1) was provided by Hangzhou Specialist Peptide Biotechnology Co. Ltd (Hangzhou, China). RPMI Medium 1640, fetal bovine serum (FBS) and 3-(4,5-dimethyl-2-thiazolyl)-2,5-diphenyl-2-H-tetrazolium bromide (MTT) were purchased from Invitrogen Corporation (Carlsbad, CA).

Preparation of nanoparticles loaded with DOX and TAN

Lipid nanoparticles loaded with DOX and TAN (N-DOX/TAN, Figure 1) were prepared by emulsification and solvent-diffusion method (Zhang, Zhu, et al., 2019). Briefly, DOX (50 mg), TAN (50 mg), and SBL (100 mg) were dissolved in acetone (10 mL) to get the organic phase. DSPE-PEG-HZ (100 mg) was suspended in water contained poloxamer 188 (1%, w/v) to form the aqueous phase. The aqueous phase was added to the organic phase dropwise under sustained ultrasound. Lipid nanoparticles loaded with DOX (N-DOX), lipid nanoparticles loaded with TAN (N-TAN) and blank nanoparticles without the drug (Blank N) were prepared by the same method.

Preparation of PSMA targeted nanoparticles loaded with DOX and TAN

PSMA targeted nanoparticles loaded with DOX and TAN (P-N-DOX/TAN, Figure 1) were synthesized by conjugating a PSMA targeted ligand (Chen et al., 2012): The acid end of P1 with the NH$_2$ end of DSPE-PEG-HZ (Figure 1). Briefly, P1, EDC (1.2 equivalents) and NHS (1.2 equivalents) were dissolved in anhydrous methylene chloride immersed in ice bath for 10 min (Chen, Zhang, et al., 2020). Then the mixture was added to N-DOX/TAN suspension under stirring (400 rpm) at room temperature for 6 h. The resulting solution was dialyzed (MWCO = 2 kDa) against distilled water for 12 h and lyophilized to get P-N-DOX/TAN. BCA protein assay kit was applied to test the absorbance of P-N-DOX/TAN and free P1
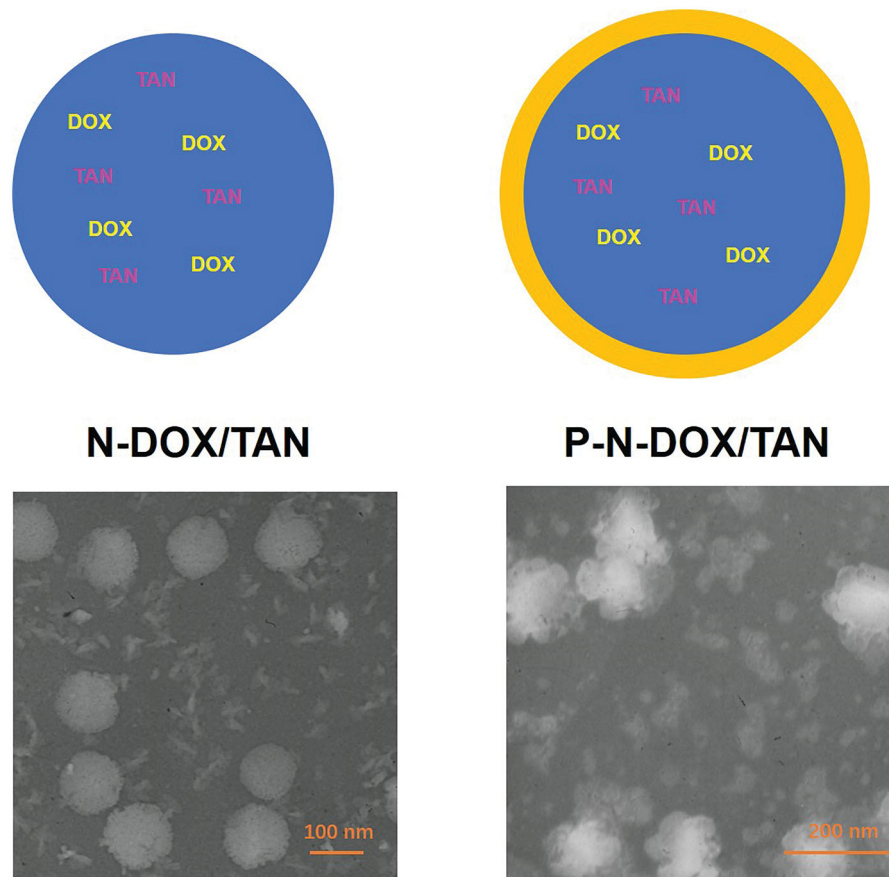

N-DOX/TAN

P-N-DOX/TAN

Figure 1. Scheme graphs and TEM images of N-DOX/TAN and P-N-DOX/TAN.

at 562 nm to evaluate if the P1 was successfully conjugated onto the nanoparticles (Guo et al., 2019). The conjugation efficiency (CE) was calculated using the following equation (Lu et al., 2019): CE (%) = (The total amount of P1 added − The amount of free P1 in the dispersion)/The total amount of P1 added × 100.

Characterization of nanoparticles

The morphology of nanoparticles was observed using transmission electron microscopy (TEM, Hitachi, Tokyo, Japan) (Li et al., 2020). The particle size, size distribution, and zeta potential were assessed by a Zetasizer Nano ZS (Malvern Instruments, Malvern, UK).

Stability of nanoparticles

The stability of nanoparticles was assessed under two different conditions and times: one is 4 °C of storage for 2 months and another is in 10% FBS in DMEM media at 37 °C for 72 h (Suh et al., 2017). Particle size changes were measured to determine stability.

Drug loading and release

The drug loading (DL) and encapsulation efficiency (EE) was measured. The amount of DOX was determined by ultraviolet absorbance with a UV spectrophotometer (Thermo Fisher Scientific, Madison, USA) at emission wavelength: 485 nm and excitation wavelength: 590 nm (Zhao et al., 2014). The amount of TAN was measured by RP-HPLC analysis at a wavelength of 253 nm (Lin et al., 2014). The EE and LC were calculated using the following equations (Hong et al., 2019): DL (%) = The amount of drugs in the nanoparticles/The amount of drugs loaded nanoparticles × 100; EE (%) = The amount of drugs in the nanoparticles/The amount of drugs in feeding solution × 100.

The release of drugs from nanoparticles was investigated using the dialysis method (Li et al., 2017). Samples were placed into dialysis bags (molecular weight cutoff of 3500 Da). Then the dialysis bags were immersed in acetate buffer at different pH values: 5.5, 6.5, and 7.4 and incubated at 37 °C with constant shaking (100 rpm). At predetermined times, 300 μL of dialysis solution was withdrawn for analysis using the methods above, and the same amount of fresh buffer was added.

Cellular uptake

Prostate cancer cell lines LNCaP cells were purchased from American Type Culture Collection (ATCC, Manassas, VA) and maintained in RPMI-1640 supplemented with 10% (v/v) fetal bovine serum at 37 °C under 5% CO_2 atmosphere.

Cellular uptake of P-N-DOX/TAN and N-DOX/TAN was evaluated using coumarin-6 (C-6) as an indicator (Fu et al., 2020). C-6 (20 mg) was added along with drugs during the preparation of nanoparticles procedure and C-6 loaded P-N-DOX/TAN and N-DOX/TAN were added to LNCaP cells and incubated for 1 h. The cell uptake efficiency was photographed by fluorescence microscopy and quantified by flow cytometry.

In vitro cytotoxicity and synergistic effect

LNCaP cells were seeded in 96-well plates at a density of 3000 cells per well. After overnight incubation, samples with different drug concentrations including drugs loaded nanoparticles, and free DOX and TAN combination (free DOX/TAN) were added separately and further cultured for 48 h. In vitro cytotoxicity of nanoparticles and free drugs was evaluated using MTT assay (Fan et al., 2015). The drug concentration causing 50% inhibition (IC_{50}) was calculated.

The synergistic effect of the system was calculated by the combination index (CI) using the Chou–Talalay method (Chou, 2010). CI when the drug concentration causing 50% inhibition (CI_{50}) was calculated by $C_{DOX}/IC_{50\text{-}DOX} + C_{TAN}/IC_{50\text{-}TAN}$ (Wang et al., 2021). C_{DOX} and C_{TAN} are the concentration of DOX and TAN in the combination system (N-DOX/TAN) at the IC_{50} value. $IC_{50\text{-}DOX}$ represents the IC_{50} value of N-DOX, and $IC_{50\text{-}TAN}$ is the IC_{50} value of N-TAN. CI <1, =1, and >1 are considered as synergism, additive, and antagonism, respectively.

In vivo tissue distribution

BALB/c nude mice (female, weighing 18–22 g) were purchased from Beijing Vital River Laboratory Animal Technology Co., Ltd. (Beijing, China), and LNCaP cells (1×10^6, 0.2 mL per mice) were injected to the right flanks of the mice to produce PCa bearing xenograft. The animal experiments were approved by the Animal Ethics Committee of the Municipal Hospital of Zaozhuang. When the tumor grew to a volume of about 100 mm³, mice were randomly divided into 3 groups (10 mice each group, totally 30 mice) and intravenously injected with P-N-DOX/TAN, N-DOX/TAN, and free DOX/TAN at a drug dose of 5 mg per kg body weight (Chen et al., 2010). At 1 h and 48 h, the tissues (tumor, heart, lung, liver, spleen, and kidney) were removed and washed with physiological solution, weighed, and homogenized. The mixture was vortexed and centrifuged (15,000 rpm, 10 min), and the supernatants were analyzed under the condition described in 'Drug loading and release' section to determine the drug distribution in vivo.

In vivo anti-tumor efficiency

PCa bearing mice were randomly divided into 7 groups (10 mice each group, totally 70 mice) and intravenously injected with P-N-DOX/TAN, N-DOX/TAN, N-DOX, N-TAN, blank N, free DOX/TAN, and 0.9% saline at a drug dose of 5 mg per kg body weight every 2 days (Du et al., 2013). Tumor volume and body weight were measured every 2 days until 18 days of study. Tumor volumes were calculated as the longest axis × the perpendicular shorter tumor axis² × 0.5. Besides body weights, other indicators including the alanine aminotransferase (ALT, the function of liver), the creatinine (CRE,
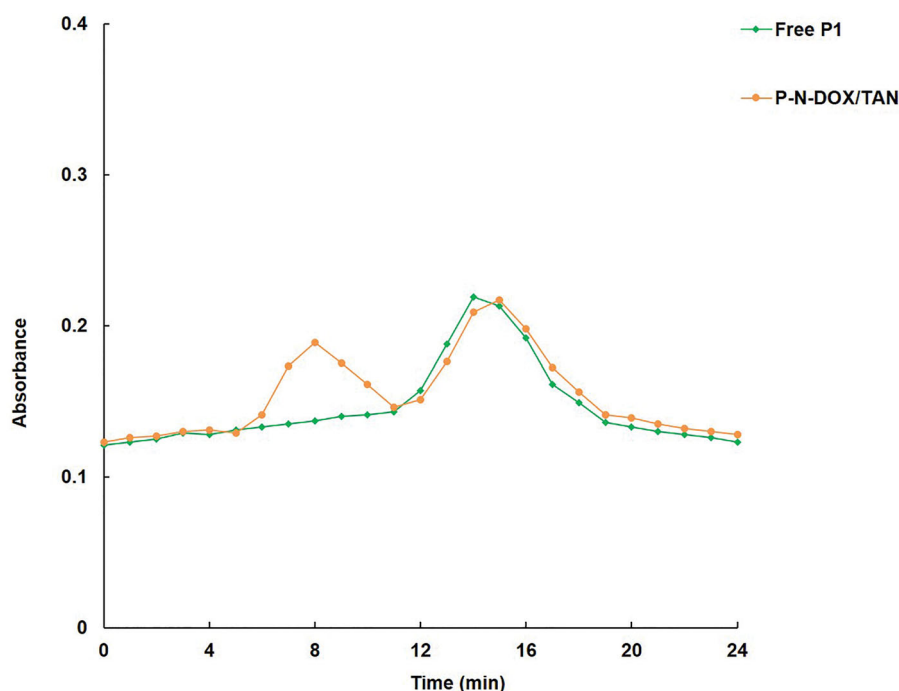
Figure 2. The absorbance curves following elution of free P1 and P-N-DOX/TAN.

Table 1. Characterization of nanoparticles.

Nanoparticles	Particle size (nm)	Size distribution	Zeta potential (mV)	DL (%) DOX	DL (%) TAN	EE (%) DOX	EE (%) TAN
Blank N	101.9 ± 3.3	0.13 ± 0.01	26.9 ± 2.1	N/A	N/A	N/A	N/A
N-DOX	99.6 ± 3.1	0.12 ± 0.02	24.3 ± 1.9	9.5 ± 1.2	N/A	91.3 ± 3.1	N/A
N-TAN	100.3 ± 2.6	0.11 ± 0.01	23.6 ± 2.3	N/A	10.7 ± 1.5	N/A	89.5 ± 2.8
N-DOX/TAN	102.5 ± 3.7	0.15 ± 0.02	25.4 ± 2.8	8.9 ± 1.1	9.6 ± 0.9	92.1 ± 3.7	90.1 ± 3.2
P-N-DOX/TAN	139.7 ± 4.1	0.16 ± 0.03	11.2 ± 1.6	8.1 ± 0.8	9.2 ± 1.0	90.9 ± 3.3	91.4 ± 3.4

the function of kidneys), and the white blood cells (WBC) were also observed (Wang et al., 2021).

TUNEL assay

Tumor tissue was sliced and detected by TUNEL assay using in situ cell death assay kit to evaluate the apoptotic cells in tumor tissue (Sun et al., 2019). Apoptotic cells were photographed under a fluorescence microscope and TUNEL-positive cells were measured with Image J Software.

Statistical analysis

Student's *t*-test was used for the statistical analysis. Data were reported as means ± standard deviation (SD) and a difference was considered statistically significant when $p < .05$.

Results

Characterization of PSMA targeted ligand conjugation

Figure 2 illustrated the absorbance curves following elution of free P1 and P-N-DOX/TAN. There is one peak from 12 to 17 min at the free P1 curve, while by contrast, there are two peaks separated at the curve of P-N-DOX/TAN. One of the peaks is overlapped with the peak of free P1, which could

be proof of PSMA targeted ligand conjugation. The conjugation efficiency (CE) was 78.9%.

Characterization of nanoparticles

TEM images showed that both P-N-DOX/TAN and N-DOX/TAN are spherical particles (Figure 1). The difference is there are coats on the surface of P-N-DOX/TAN, which could be proof of the ligand modification. The sizes of P-N-DOX/TAN and non-modified nanoparticles were around 140 nm and 100 nm, respectively (Table 1). This may be explained by the surface coating of P1 that enlarged the particle size. Also if we observe the zeta potential, it decreased from 25.4 to 11.2 mV after modification (Table 1). The increase in size with a clear coat on the TEM images and decrease of surface charge could suggest the successful preparation of P-N-DOX/TAN. Table 1 also summarized the DL and EE of the nanoparticles.

Stability and drug release of nanoparticles

Figure 3 showed the size variations during 2 months of storage and in the presence of serum. The sizes of nanoparticles remained unchanged during 2 months at 4 °C (Figure 3(A)), indicating the systems were stable in this storage condition. Also, during 72 h of study in the serum, nanoparticles
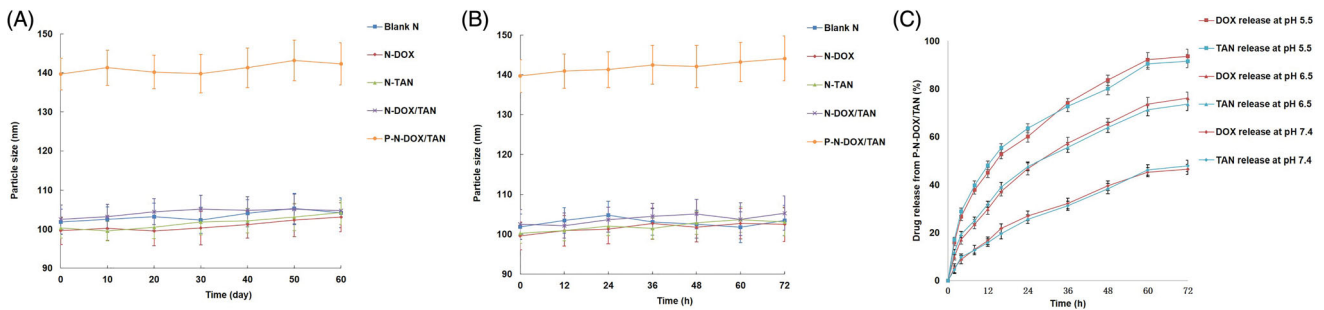
Figure 3. The size variations in the presence of serum (A), during 2 months of storage (B), and release of drugs from nanoparticles at different pH values (C). Data presented as means ± SD.

N-DOX/TAN

P-N-DOX/TAN

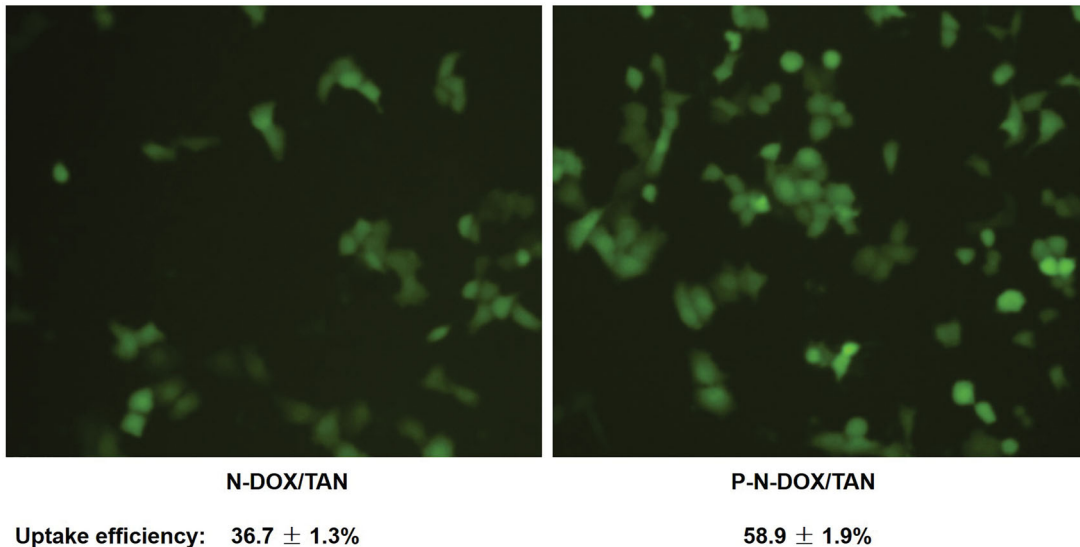Uptake efficiency: 36.7 ± 1.3%

58.9 ± 1.9%

Figure 4. Cellular uptake efficiency of N-DOX/TAN and P-N-DOX/TAN.

showed no significant increase or decrease of sizes (Figure 3(B)), which may be evidence of the stability of the systems for intravenous injection. The release of DOX and TAN from P-N-DOX/TAN was much faster at pH 5.5 than at pH 6.5, the latter is also faster than at pH 7.4 (Figure 3(C)). At pH 5.5 and 6.5, over 90% and nearly 80% of drugs were released at the end of the study, while at pH 7.4, the data was above 50%.

Cellular uptake

P-N-DOX/TAN and N-DOX/TAN illustrated different cellular uptake efficiency as showed in florescence images (Figure 4). P-N-DOX/TAN achieved higher uptake by LNCaP cells (58.9 ± 1.9%) than N-DOX/TAN (36.7 ± 1.3%), which may attribute to the modification of PSMA targeted ligand.

In vitro *cytotoxicity and synergistic effect*

The cytotoxicity of P-N-DOX/TAN was remarkably higher than that of N-DOX/TAN ($p < .05$), the latter showed significant cancer cell inhibition ability compared with N-DOX and N-TAN (Figure 5(A)). Blank nanoparticles had no obvious influence on cell viability, which was similar to the saline control group. To evaluate the synergistic effect of DOX and TAN

loaded in nanoparticles, CI values were analyzed using the CI50 parameters of N-DOX/TAN, N-DOX, and N-TAN. The DOX to TAN ratios were set from 1:4 to 4:1 (w/w). Figure 5(B) revealed that when DOX: TAN was 1:1 (w/w), the most obvious synergistic effect was observed with all CI values <1.

In vivo *tissue distribution and anti-tumor efficiency*

P-N-DOX/TAN showed the most remarkable drug accumulation in the tumor at 48 h of study, which is higher than that of N-DOX/TAN and free DOX/TAN ($p < .05$) (Figure 6). At 1 h, drugs loaded nanoparticles distributed less in the kidney than free drugs ($p < .05$). Figure 7(A) illustrated the antitumor efficiency of all kinds of samples tested. P-N-DOX/TAN exhibited the most significant tumor inhibition efficiency, higher than that of N-DOX/TAN and other formulations ($p < .05$). N-DOX/TAN also presented more inhibition effects on tumor growth than N-DOX and N-TAN ($p < .05$). The body weight changes were summarized in Figure 7(B). The drugs contained nanoparticles groups caused no obvious body weight change, while free DOX/TAN reduced the body weight during the test time. The blank nanoparticles and saline control groups also exhibited a reduction in body weight. Drugs loaded nanoparticles showed no significant change on ALT, CRE, and WBC, while an increase of CRE was observed in the
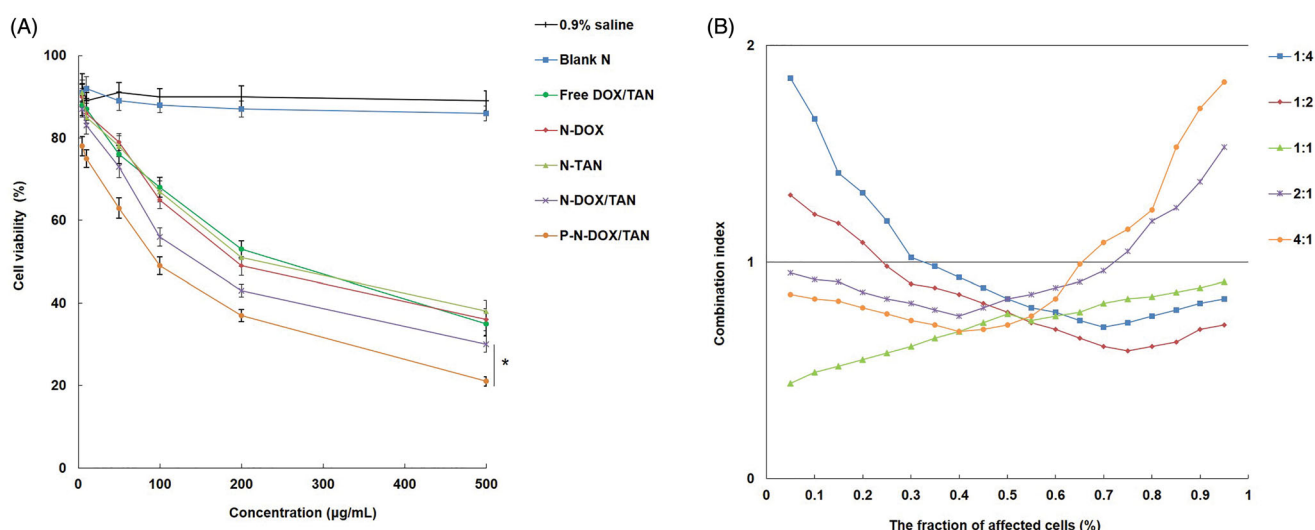
Figure 5. *In vitro* cytotoxicity of nanoparticles and free drugs evaluated using MTT assay (A), and combination index (CI) calculation. Data presented as means ± SD. *p < .05.
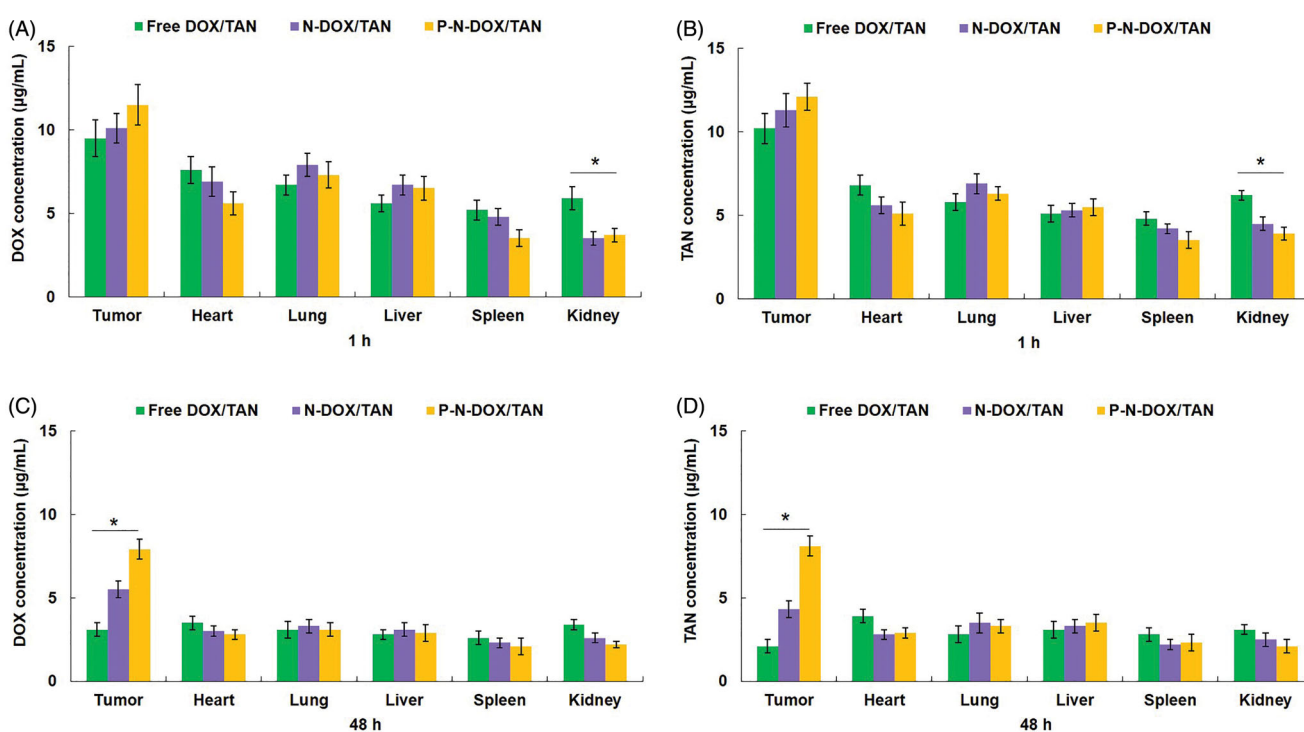

Figure 6. *In vivo* tissue distribution of DOX (A) and TAN (B) at 1 h; DOX (C) and TAN (D) distribution at 48 h. Data presented as means ± SD. *p < .05.

free drugs group (Figure 8). TUNEL assay showed that the TUNEL-positive cells ratio of P-N-DOX/TAN group was higher than other groups (Figure 9, *p < .05*), also drugs loaded nanoparticles exhibited better efficiency on the apoptosis of cells than the free drugs (*p < .05*).

Discussion

The aim of this study is (1) to carry dual drugs: DOX and TAN to achieve synergetic antitumor efficiency. (2) To modify the system with PSMA targeted ligand and also bring pH-sensitive ability through adipic acid dihydrazide (HZ) linker. To achieve the first purpose, N-DOX/TAN was prepared by

emulsification and solvent-diffusion method. N-DOX/TAN showed a spherical shape, a size of 102.5 ± 3.7 nm, and a zeta potential of 25.4 ± 2.8 mV. When modified with PSMA targeted ligand (P-N-DOX/TAN), the TEM images showed a coat on the surface of particles and increased size (139.7 ± 4.1 nm), and reduced zeta potential (11.2 ± 1.6 mV). Both P-N-DOX/TAN and N-DOX/TAN were determined stable during 2 months of storage and in the presence of serum, indicating the stability of the nanoparticles for injection and storage conditions.

To evaluate the pH sensitivity of the nanoparticles, the release mediums at pH 5.5, 6.5, and 7.4 were applied. The release profiles showed that the drug release from P-N-DOX/TAN was more sufficient at lower pH values. The results
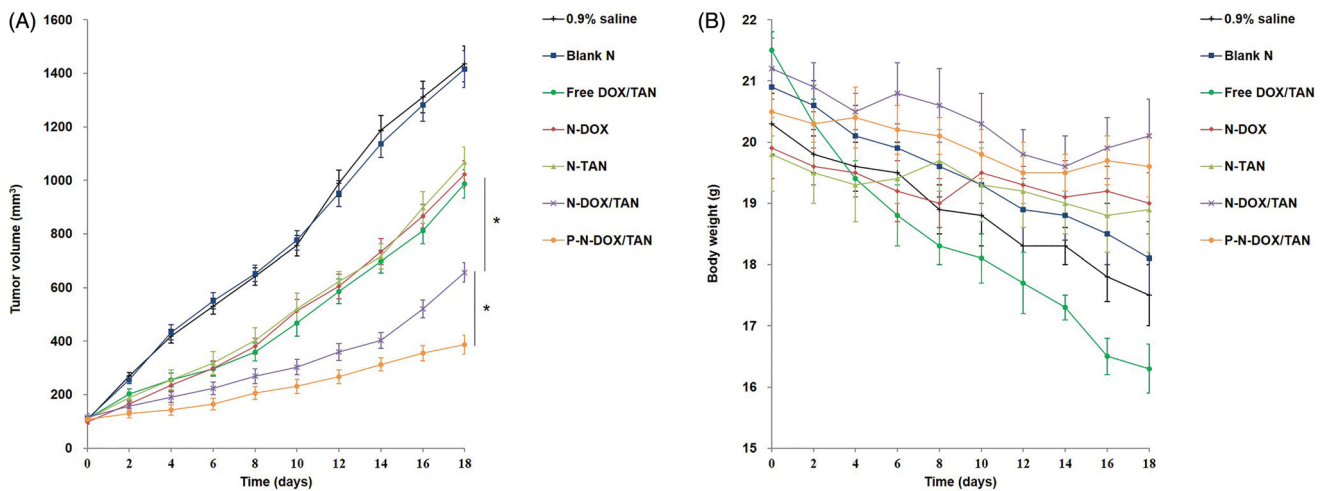
Figure 7. *In vivo* anti-tumor efficacy (A) and body weight changes (B) during treatment. Data presented as means ± SD. $*p < .05$.
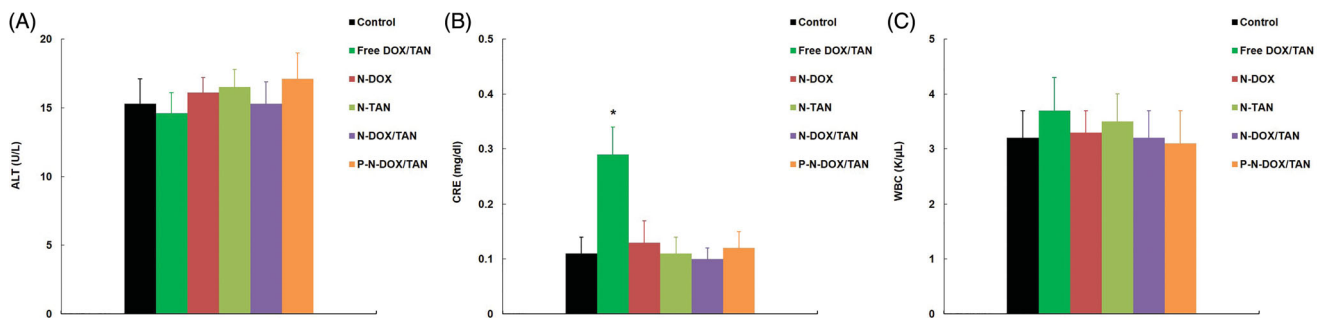

Figure 8. The data of ALT (A), CRE (B) and WBC (C). Data presented as means ± SD. $*p < .05$.

suggest the pH dependence of N-DOX/TAN which may attribute to the cleavage of pH-responsive linker that lets the drugs be released more from the nanoparticles (Men et al., 2020). Tumor tissue is reported to have a low pH (pH 6.5) and an intracellular microenvironment of pH 5.5 (Yugui et al., 2019). So the P-N-DOX/TAN may release more sufficiently in the tumor site. Cancer cell internalization and retention ability of nanoparticles have a strong impact on the therapeutic effects (Lin et al., 2014), which could be observed by the cellular uptake efficiency of the nanoparticles. P-N-DOX/TAN achieved higher uptake by LNCaP cells (58.9 ± 1.9%) than N-DOX/TAN (36.7 ± 1.3%), which may attribute to the modification of PSMA targeted ligand. Higher internalization of the drugs loaded nanoparticles into the cancer cells could lead to better cell growth inhibition efficacy, which may help with the *in vivo* tumor accumulation and antitumor ability (Chen, Deng, et al., 2020).

Cytotoxicity of nanoparticles was evaluated in prostate-specific membrane antigen (PSMA) positive LNCaP cells (Liu et al., 2018). Blank nanoparticles showed negligible cytotoxicity, which may be explained by the main composition of lipid nanoparticles and the systems were safe as drug delivery systems as reported by Liu et al. (2018). Evaluation of the synergistic effects in the combination drug delivery system is interesting in drugs loaded systems and a combination index (CI) was introduced for quantification of synergistic or antagonistic effect (Wang, 2020). The results illustrated that when

DOX: TAN was 1:1 (w/w), the most obvious synergistic effect was observed in the dual-drug-loaded nanoparticles and could develop the ability of the drugs to a large extent as also suggested by Zhang, Ru, et al. (2017).

In vivo biodistribution study results exhibited long-circulating characteristics of nanoparticles (Zhang, Zhang, et al., 2019). P-N-DOX/TAN showed the highest tumor tissue distribution at 48 h of study, and also exhibited the most significant tumor inhibition efficiency. The in vivo tumor inhibition effect of P-N-DOX/TAN was higher than that of N-DOX/TAN, which is in accordance with the founding of Ding et al. (2020). They found that modified nanoparticles showed improved anti-tumor efficacy than non-modified ones, suggesting the targeted therapy ability of the system. This is consistent with the observation of cellular uptake efficacy and *in vitro* cytotoxicity results that P-N-DOX/TAN could better influence tumor growth. N-DOX/TAN also presented more inhibition effect on tumor growth than N-DOX and N-TAN, which is consistent with the previous *in vitro* cytotoxicity and synergistic results and successfully highlighting the advantages of combing the DOX and TAN in one system for the PCa treatment as also illustrated by Yin et al. (2020). Bodyweight variations and other parameters were calculated to evaluate the systemic toxicity of different systems (Cui et al., 2017). No obvious change in body weight, ALT, CRE, and WBC proved the low systemic toxicity of the nanoparticles.
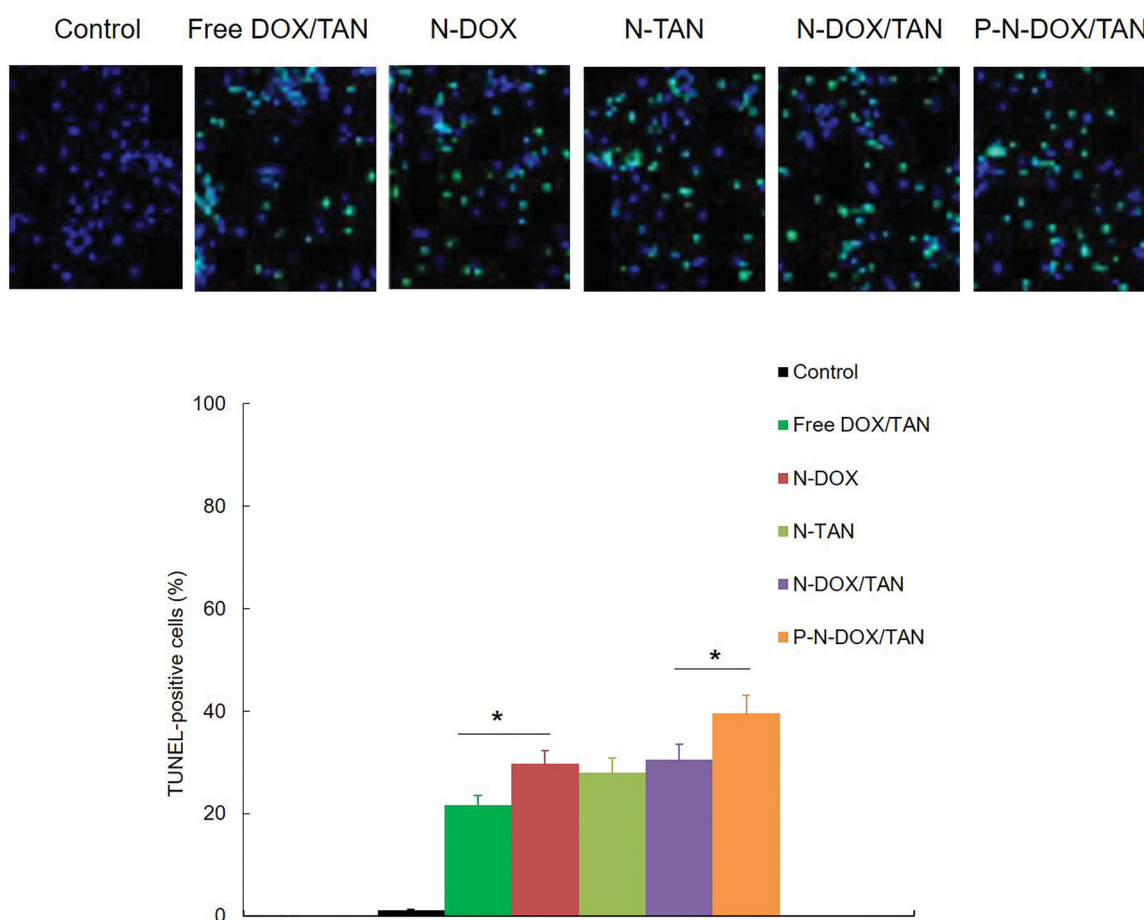
Figure 9. TUNEL assay showed the TUNEL-positive cells. Data presented as means ± SD. *$p < .05$.

Conclusion

PSMA targeted nanoparticles: P-N-DOX/TAN is constructed. It has a size of 139.7 ± 4.1 nm and zeta potential of 11.2 ± 1.6 mV. The drug release of DOX and TAN from P-N-DOX/TAN was much faster than that of N-DOX/TAN. N-DOX/TAN presented more inhibition effect on tumor growth than N-DOX and N-TAN, which is consistent with the synergistic results and successfully highlighting the advantages of combing the DOX and TAN in one system. P-N-DOX/TAN achieved higher uptake by LNCaP cells (58.9 ± 1.9%), highest tumor tissue distribution, and the most significant tumor inhibition efficiency, which can be applied as a novel drug delivery system for the PCa treatment.

Disclosure statement

No potential conflict of interest was reported by the author(s).

References

Argenziano M, Lombardi C, Ferrara B, et al. (2018). Glutathione/pH-responsive nanosponges enhance strigolactone delivery to prostate cancer cells. Oncotarget 9:35813–29.

Autio KA, Dreicer R, Anderson J, et al. (2018). Safety and efficacy of BIND-014, a docetaxel nanoparticle targeting prostate-specific membrane antigen for patients with metastatic castration-resistant prostate cancer: a phase 2 clinical trial. JAMA Oncol 4:1344–51.

Cao C, Wang Q, Liu Y. (2019). Lung cancer combination therapy: doxorubicin and β-elemene co-loaded, pH-sensitive nanostructured lipid carriers. Drug Des Devel Ther 13:1087–98.

Center MM, Jemal A, Lortet-Tieulent J, et al. (2012). International variation in prostate cancer incidence and mortality rates. Eur Urol 61:1079–92.

Chang SS, O'Keefe DS, Bacich DJ, et al. (1999). Prostate-specific membrane antigen is produced in tumor-associated neovasculature. Clin Cancer Res 5:2674–81.

Chen D, Jiang X, Liu J, et al. (2010). In vivo evaluation of novel pH-sensitive mPEG-Hz-Chol conjugate in liposomes: pharmacokinetics, tissue distribution, efficacy assessment. Artif Cells Blood Substit Immobil Biotechnol 38:136–42.

Chen G, Zhang Y, Deng H, et al. (2020). Pursuing for the better lung cancer therapy effect: Comparison of two different kinds of hyaluronic acid and nitroimidazole co-decorated nanomedicines. Biomed Pharmacother 125:109988.

Chen Y, Deng Y, Zhu C, Xiang C. (2020). Anti prostate cancer therapy: aptamer-functionalized, curcumin and cabazitaxel co-delivered, tumor targeted lipid-polymer hybrid nanoparticles. Biomed Pharmacother 127:110181.

Chen Z, Penet MF, Nimmagadda S, et al. (2012). PSMA-targeted theranostic nanoplex for prostate cancer therapy. ACS Nano 6:7752–62.

Chou TC. (2010). Drug combination studies and their synergy quantification using the Chou-Talalay method. Cancer Res 70:440–6.

Cui T, Zhang S, Sun H. (2017). Co-delivery of doxorubicin and pH-sensitive curcumin prodrug by transferrin-targeted nanoparticles for breast cancer treatment. Oncol Rep 37:1253–60.

Ding Z, Wang D, Shi W, et al. (2020). In vivo targeting of liver cancer with tissue- and nuclei-specific mesoporous silica nanoparticle-based nanocarriers in mice. Int J Nanomed 15:8383–400.

Du C, Deng D, Shan L, et al. (2013). A pH-sensitive doxorubicin prodrug based on folate-conjugated BSA for tumor-targeted drug delivery. Biomaterials 34:3087–97.

Fan X, Zhao X, Qu X, Fang J. (2015). pH sensitive polymeric complex of cisplatin with hyaluronic acid exhibits tumor-targeted delivery and improved in vivo antitumor effect. Int J Pharm 496:644–53.

Fu Q, Wang J, Liu H. (2020). Chemo-immune synergetic therapy of esophageal carcinoma: trastuzumab modified, cisplatin and fluorouracil co-delivered lipid-polymer hybrid nanoparticles. Drug Deliv 27:1535–43.

Guo S, Zhang Y, Wu Z, et al. (2019). Synergistic combination therapy of lung cancer: cetuximab functionalized nanostructured lipid carriers for the co-delivery of paclitaxel and 5-Demethylnobiletin. Biomed Pharmacother 118:109225.

Holzbeierlein J, Lal P, LaTulippe E, et al. (2004). Gene expression analysis of human prostate carcinoma during hormonal therapy identifies androgen-responsive genes and mechanisms of therapy resistance. Am J Pathol 164:217–27.

Hong Y, Che S, Hui B, et al. (2019). Lung cancer therapy using doxorubicin and curcumin combination: targeted prodrug based, pH sensitive nanomedicine. Biomed Pharmacother 112:108614.

Karantanos T, Corn PG, Thompson TC. (2013). Prostate cancer progression after androgen deprivation therapy: mechanisms of castrate resistance and novel therapeutic approaches. Oncogene 32:5501–11.

Ketola K, Viitala M, Kohonen P, et al. (2016). High-throughput cell-based compound screen identifies pinosylvin methyl ether and tanshinone IIA as inhibitors of castration-resistant prostate cancer. J Mol Biochem 5:12–22.

Li C, Li H, Wang Q, et al. (2017). pH-sensitive polymeric micelles for targeted delivery to inflamed joints. J Control Release 246:133–41.

Li D, Cui R, Xu S, Liu Y. (2020). Synergism of cisplatin-oleanolic acid co-loaded hybrid nanoparticles on gastric carcinoma cells for enhanced apoptosis and reversed multidrug resistance. Drug Deliv 27:191–9.

Li K, Zhan W, Chen Y, et al. (2019). Docetaxel and doxorubicin codelivery by nanocarriers for synergistic treatment of prostate cancer. Front Pharmacol 10:1436.

Li N, Xie X, Hu Y, et al. (2019). Herceptin-conjugated liposomes co-loaded with doxorubicin and simvastatin in targeted prostate cancer therapy. Am J Transl Res 11:1255–69.

Lin J, Wang X, Wu Q, et al. (2014). Development of salvianolic acid B-tanshinone II A-glycyrrhetinic acid compound liposomes: formulation optimization and its effects on proliferation of hepatic stellate cells. Int J Pharm 462:11–8.

Liu J, Cheng H, Han L, et al. (2018). Synergistic combination therapy of lung cancer using paclitaxel- and triptolide-coloaded lipid-polymer hybrid nanoparticles. Drug Des Devel Ther 12:3199–209.

Lu X, Liu S, Han M, et al. (2019). Afatinib-loaded immunoliposomes functionalized with cetuximab: a novel strategy targeting the epidermal growth factor receptor for treatment of non-small-cell lung cancer. Int J Pharm 560:126–35.

Men W, Zhu P, Dong S, et al. (2020). Layer-by-layer pH-sensitive nanoparticles for drug delivery and controlled release with improved therapeutic efficacy in vivo. Drug Deliv 27:180–90.

Mohler JL, Gregory CW, Ford OH, 3rd, et al. (2004). The androgen axis in recurrent prostate cancer. Clin Cancer Res 10:440–8.

Siegel R, DeSantis C, Virgo K, et al. (2012). Cancer treatment and survivorship statistics, 2012. CA Cancer J Clin 62:220–41.

Silver DA, Pellicer I, Fair WR, et al. (1997). Prostate-specific membrane antigen expression in normal and malignant human tissues. Clin Cancer Res 3:81–5.

SreeHarsha N, Maheshwari R, Al-Dhubiab BE, et al. (2019). Graphene-based hybrid nanoparticle of doxorubicin for cancer chemotherapy. Int J Nanomed 14:7419–29.

Suh MS, Shen J, Kuhn LT, Burgess DJ. (2017). Layer-by-layer nanoparticle platform for cancer active targeting. Int J Pharm 517:58–66.

Sun N, Wang D, Yao G, et al. (2019). pH-dependent and cathepsin B activable CaCO3 nanoprobe for targeted in vivo tumor imaging. Int J Nanomed 14:4309–17.

Tambe P, Kumar P, Paknikar KM, Gajbhiye V. (2018). Decapeptide functionalized targeted mesoporous silica nanoparticles with doxorubicin exhibit enhanced apoptotic effect in breast and prostate cancer cells. Int J Nanomed 13:7669–80.

Wang B, Hu W, Yan H, et al. (2021). Lung cancer chemotherapy using nanoparticles: enhanced target ability of redox-responsive and pH-sensitive cisplatin prodrug and paclitaxel. Biomed Pharmacother 136:111249.

Wang J. (2020). Combination treatment of cervical cancer using folate-decorated, pH-sensitive, carboplatin and paclitaxel co-loaded lipid-polymer hybrid nanoparticles. Drug Des Devel Ther 14:823–32.

Wang X, Huang SS, Heston WD, et al. (2014). Development of targeted near-infrared imaging agents for prostate cancer. Mol Cancer Ther 13:2595–606.

Wang M, Zeng X, Li S, et al. (2019). A novel tanshinone analog exerts anti-cancer effects in prostate cancer by inducing cell apoptosis, arresting cell cycle at G2 phase and blocking metastatic ability. Int J Mol Sci 20:4459.

Xu C, Song RJ, Lu P, et al. (2018). pH-triggered charge-reversal and redox-sensitive drug-release polymer micelles codeliver doxorubicin and triptolide for prostate tumor therapy. Int J Nanomed 13:7229–49.

Yin N, Yu H, Zhang X, Lv X. (2020). Enhancement of pancreatic cancer therapy efficacy by type-1 matrix metalloproteinase-functionalized nanoparticles for the selective delivery of gemcitabine and erlotinib. Drug Des Devel Ther 14:4465–75.

Yugui F, Wang H, Sun D, Zhang X. (2019). Nasopharyngeal cancer combination chemoradiation therapy based on folic acid modified, gefitinib and yttrium 90 co-loaded, core-shell structured lipid-polymer hybrid nanoparticles. Biomed Pharmacother 114:108820.

Zhang HW, Dang Q, Zhang ZW, Wu FS. (2017). Development, characterization and evaluation of doxorubicin nanostructured lipid carriers for prostate cancer. J BUON 22:102–11.

Zhang L, Zhu K, Zeng H, et al. (2019). Resveratrol solid lipid nanoparticles to trigger credible inhibition of doxorubicin cardiotoxicity. Int J Nanomed 14:6061–71.

Zhang R, Ru Y, Gao Y, et al. (2017). Layer-by-layer nanoparticles co-loading gemcitabine and platinum (IV) prodrugs for synergistic combination therapy of lung cancer. Drug Des Devel Ther 11:2631–42.

Zhang Y, Zhang P, Zhu T. (2019). Ovarian carcinoma biological nanotherapy: comparison of the advantages and drawbacks of lipid, polymeric, and hybrid nanoparticles for cisplatin delivery. Biomed Pharmacother 109:475–83.

Zhao X, Chen Q, Liu W, et al. (2014). Codelivery of doxorubicin and curcumin with lipid nanoparticles results in improved efficacy of chemotherapy in liver cancer. Int J Nanomed 10:257–70.